Analyst

Accepted Manuscript

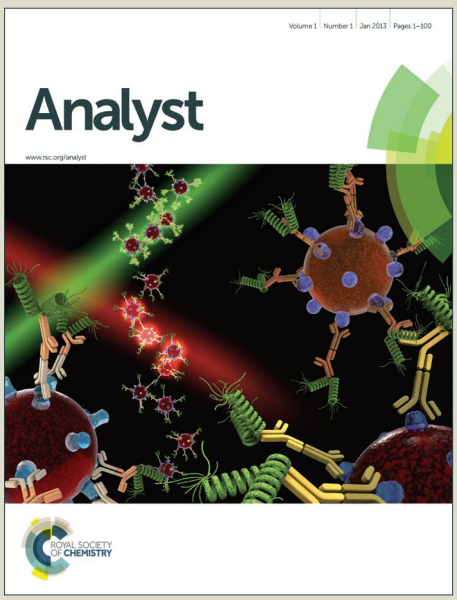

ROYAL SOCIETY OF CHEMISTRY

www.rsc.org/analyst

Analyst

ARTICLE

A simple interfacial pH detection method for cationic amphiphilic self-assemblies utilizing a Schiff-base molecule

Received 00th January 20xx,
Accepted 00th January 20xx

DOI: 10.1039/x0xx00000x

www.rsc.org/

Yeasmin Sarkar,[a] Sanju Das,[a,b] Ambarish Ray,[b] Suresh Kumar Jewrajka,[c] Shun Hirota[d] and Partha Pratim Parui*[a]

A simple pH-sensing method for cationic micelle and vesicle interfaces is introduced, utilizing a Schiff-base molecule, 2-((4H-1,2,4-triazol-4-ylimino)methyl)-6-(hydroxymethyl)-4-methylphenol (AH). AH containg a phenolic moiety was obtained by the reaction between 4-amino-4H-1,2,4-triazole containg polar O- and N-centres with opposite polarity to the cationic interface and 2-hydroxy-3-(hydroxymethyl)-5-methylbenzaldehyde. Acid/base equilibrium of AH was investigated at the interfaces of cetrimonium bromide (CTAB) micelles, tri-block-copolymeric micelles (TBPs) and large unilamellar vesicles (LUVs) of different lipid compositions using steady state UV-Vis absorption spectroscopy. AH interacted strongly with the micelle and vesicle interfaces, according to the binding studies with LUV. Larger amount of AH proton dissociation was observed when it was localized at the interface of micelles and vesicles compared to that in the bulk phase, indicating that the pH value at the cationic interfaces are higher than that in the bulk phase. The pH values were about 2.2 and 1.6 units higher at the CTAB and TBP micelle interfaces, respectively, than the bulk pH. The pH variation decreased from 2.4 to 1.5 unit by increasing the neutral 1,2-dioleoyl-sn-glycero-3-phosphocholine (DOPC) lipid content from 0 to 50% in the cationic dimethyldioctadecylammonium (DDAB) LUV, indicating that the interfacial positive charges are responsible for the higher interfacial pH. Detailed structural and absorption characters of neutral AH and its anionic A^- forms were investigated by fluorescence spectroscopic measurements and DFT based theoretical calculations. The present simple pH detection method may be applied to various biological micelle and vesicle interfaces.

Introduction

Cellular interface plays a pivotal role in a many fundamental biological processes, such as metabolism,[1-4] enzyme catalysis,[5] cell apoptosis,[6-9] transport of small peptides[10] and organelles,[11] cell signalling and membrane trafficking,[11] ion channel formation[12] and various signalling pathways. Cellular interface, known as biological membrane, contains lipid bilayers as its basic structural unit. Such bilayers form boundaries between intracellular cytoplasm and the cell's outside environment, as well as between cytoplasm and the interior of many cell's organelles. It has been shown that the membrane structural change is induced by a minute alteration of the interfacial pH, causing cellular dysfunction, which may be associated with sever diseases like cancer,[13-15] Alzheimer's disease etc.[16] The interface localized amyloid precursor protein (APP) which is widely believed to be related to the aetiology of Alzheimer's disease, can adopt different conformations depending on the local proton concentration.[17] It has recently been reported that pH dependent transfer of peptide nano-pore into the cancer cell membranes can induce the apoptosis process.[18] The functions of various membrane bound proteins are highly sensitive to the environmental pH.[19] Some proteins, such as ATP synthase, may manipulate the proton concentration at the membrane interface.[20] On the other hand, cationic lipid bilayer vesicles and micelles have promising applications, including targeted drug-delivery devices, biosensors and nanoreactors.[21-25] For targeted drug delivery, the drugs may penetrate and electrostatically anchor to the cationic lipid self-assembled systems, and be released by the interaction with negatively charged outer cellular interfaces at a well-defined location in a controlled manner as a function of interfacial or intracellular pH of the medium.[24] Therefore, accurate detection of the interfacial pH is indispensable for identification of various biochemical events which are controlled by the interfacial pH of the cellular membranes.

Recently, several investigations have suggested a discrepancy in interfacial pH from the bulk pH in various micellar systems, due to micro-heterogeneous compartmentalization.[26-33] However, quantitative estimation of the interfacial pH in these systems has rarely been addressed. Identification of pH at such bilayer interfaces is extremely difficult, due to the complexity and micro-heterogeneous nature of the membrane. Recently, Tahara and co-workers have developed a heterodyne-detected electronic sum

[a] Department of Chemistry, Jadavpur University, Kolkata 700032, India. Fax: +91-33-24146223, Phone:+91-9433490492,E-mail: parthaparui@yahoo.com
[b] Department of Chemistry, Maulana Azad College, Kolakta 700013, India.
[c] CSIR-Central Salt & Marine Chemicals Research Institute, Gujarat-364002, India.
[d] Graduate School of Materials Science, Nara Institute of Science and Technology, Nara 630-0192, Japan.
Electronic Supplementary Information (ESI) available: For additional spectroscopic and synthetic information. See DOI: 10.1039/x0xx00000x

frequency generation (HD-ESFG) spectroscopic method to investigate the acid/base equilibrium at cetrimonium bromide (CTAB) micelles and lipid vesicles, and monitored the interfacial pH values. They have shown that the interfacial pH is substantially altered from the bulk pH.[34,35]

In the present study, a simple method is developed for accurate interfacial pH evaluation of various biologically related systems, such as CTAB micelles, large unilamellar vesicles (LUVs) of single lipids or mixture of different types of lipids and block copolymer core-shell type micelles. A pH probe which localizes at the cationic interface was designed to eliminate the contribution of the bulk phase. The pH dependent acid/base equilibrium of the probe at the interface was monitored to assess the interfacial pH value. The deviation of the interfacial pH from the bulk pH in the CTAB micellar system was close to the value reported by the HD-ESFG method. The present simple UV-Vis spectrometric method utilizing a Schiff-base molecule is suitable for accurate estimation of interfacial pH values in membrane systems.

Experimental

General experimental methods

Unless otherwise mentioned, all required chemicals and solvents of purest grade were purchased from Sigma-Aldrich Chemicals Private Limited and were used without further purification. Milli-Q Millipore®18.2 MΩ cm water was used for buffer solutions and other spectroscopic samples. Different 20 mM buffer compositions were used for UV-Vis absorption and fluorescence samples to achieve specific pH within pH 5.5–12.0: cacodylate for 5.5–7.0, tris-HCl for 7.0–9.0 and carbonate/bicarbonate for 9.0–12.0. The pH of the buffer was adjusted by an addition of required amount of either ~ 1.0 M NaOH or 1.0 M HCl solution, monitored with a Systronics digital pH meter (Model No. 335). For spectroscopic studies, AH was mixed with a required amount of different analytes in 20 mM of specific buffer, with adjustment of the final pH value with an addition of either 0.1 M NaOH or 0.1 M HCl if required. ^{1}H- and ^{13}C- NMR spectra were performed in DMSO-d_6 with a Bruker 300-MHz NMR spectrophotometer using tetramethylsilane (δ = 0) as an internal standard.

The triblock copolymer, containing poly(methyl methacrylate) central block (PMMA) and poly(2-dimethylaminoethyl) methacrylate end block (PDMA), with molecular weight of (M_n) ~ 28 kD and a polydispersity index (PDI) of 1.20 was synthesized by two step atom transfer radical polymerization as reported earlier.[36] The tertiary amino groups were subjected to quaternization by butyl bromide (see ESI for synthesis details).

Synthesis of Schiff-base molecule

2-hydroxy-3-(hydroxymethyl)-5-methylbenzaldehyde (HHMB) was synthesized according to our published procedure.[37] The detailed synthetic procedures for the Schiff-base molecule, 2-((4H-1,2,4-triazol-4-ylimino)methyl)-6-(hydroxymethyl)-4-methylphenol (AH) were mentioned elsewhere.[38] In brief, 4-Amino-4H- 1,2,4-triazole (Tz) (0.084 g, 1 mmol) was added drop-wise to a methanolic solution

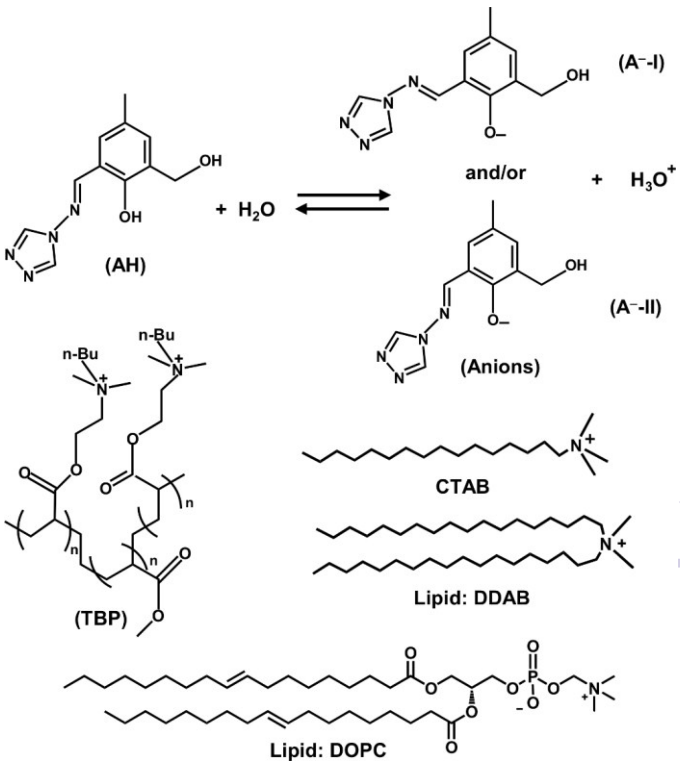

Scheme 1. Schematic views of (upper panel) acid/base equilibrium of the Schiff-base molecule AH and (lower panel) cationic amphiphilic self-assembled systems.

of HHMB (0.166 g, 1 mmol) by constant stirring, and 2 drops of acetic acid were further added to the solution. The mixture was refluxed for 2 h and subsequently filtered. The filtrate was evaporated under reduced pressure to obtain the crude product. The product was purified by column chromatography, followed by rotary evaporation. The obtained solid product was dried over P_2O_5 under vacuum. The Schiff-base molecule (AH) was further recrystallized from a toluene-chloroform mixed solvent (7:3, v/v) to afford yellow colored crystals. The structural analyses were performed by ESI-MS$^+$, ^{1}H-NMR and ^{13}C-NMR measurements (Figs. S1 and S2, ESI). ESI-MS$^+$ for AH in water: m/z Cal for [AH+H]$^+$: 233.2420; Found: 233.0276 (For details, see mass spectrum in ESI, S6). ^{1}H NMR (DMSO-d_6, 300MHz): δ = 2.27 (s, 3H, $ArCH_3$), 4.56 (d, 2H, $–CH_2$), 5.20 (t, 1H, alcoholic-OH, J = 2), 7.32 (s, 1 H, ArH), 7.36 (s, 1H, ArH), 9.15 (s, 3H, imine-H and triazole ring-H), 9.93 (s, 1H, ArOH) ppm. ^{13}C NMR (DMSO-d_6, 75 MHz): 20.54, 58.44, 117.07, 128.72, 129.19, 130.73, 132.93, 139.24, 153.43, 158.79 ppm (For details, see NMR spectra in ESI, S5).

Large unilamellar vesicle (LUV) preparation

Appropriate amount of dimethyldioctadecylammonium bromide (DDAB), 1,2-dioleoyl-sn-glycero-3-phosphocholine (DOPC) or their mixture was dissolved in 1 mL chloroform. Thin lipid film on the wall of a round bottom flask was prepared with a rotary evaporator by removing the chloroform solvent at room temperature. Residual amount of chloroform in the thin lipid film was completely removed *in vauco* for 3 h. Appropriate 20 mM buffer solution was added to the lipid film at 40°C for hydration of the film. The aqueous lipid

solution was vortexed 2 min for complete dissolution of the lipids. Five cycles of freeze-and-thaw were performed between –196 and 50°C. To obtain large unilamellar vesicles (LUVs), the liposome dispersion was extruded 15 times through two stacked polycarbonate membrane filters with different pore sizes (50, 100 and 200 nm) equipped in a Liposo Fast mini extruder (Avestin). For spectroscopic measurements, the resultant LUV solution was diluted with appropriate amount of buffer to definite lipid concentration.

UV-Vis absorption and fluorescence studies

UV-Vis optical absorption and fluorescence spectra were monitored in 20 mM buffer at 27°C with a UV-2450 spectrophotometer (Shimadzu, Japan) and Perkin Elmer LS-55 spectro-fluorimeter (Perkin Elmer, USA), respectively. Quartz cells with 1-cm path-lengths were used for absorption and fluorescence measurements, respectively. Spectro-fluorimeter equipped with an excitation and emission automatic polarizer was used for fluorescence anisotropic measurements. Fluorescence transient decays were monitored with time-correlated-single-photon-counting (TCSPC) techniques. Two separate nanosecond diodes with excitation at 370 and 450 nm, respectively (nano-LED; IBH, U. K.), were used as the light source. A TBX4 detection module (IBH, U. K.) coupled with a special Hamamastu photomultiplier tube (PMT) was used for the detection of the fluorescence decays. The solutions for analysis were passed through a 0.45 mm filter (Millex, Millipore) before the measurements. All measurements were repeated at least three times to check the reproducibility.

Binding studies

The LUV of different lipid composition (2.5 mM) in 20 mM buffer solution (pH 6.0 or 8.0) containing 5.0 µM AH was incubated for 30 min. A 100K MW cut-off centrifugal mini-filter (Amicon Ultra-0.5 mL Centrifugal Filters, Millipore) was used to collect the unbound AH in the bulk phase. Approximately 200 µL of the filtrate was collected from the initial 400 µL lipid solution after centrifugation for about 2 min at 5000 g. The amount of residual AH in the filtrate was estimated by the UV-Vis absorption spectra, and the amount of unbound AH was calculated (See ESI for details).

Theoretical calculations

Density functional theory (DFT) and time-dependent DFT (TD-DFT) calculations were performed using the Gaussian 09 program.[39] Geometry optimization based on the most probable structure for AH and its two anionic conformers A^--I and A^--II was performed using B3LYP exchange-correlation function. The 6-31G++(d,p) basis set for atoms and the geometries was optimized in gas phase. The global minima of all the species were confirmed by the positive vibrational frequencies. To investigate the electronic properties of the singlet excited state in water, TD-DFT calculation was applied using the optimized geometries of the ground states (S_0) for respective species in aqueous solution by adapting the conductor polarized continuum model (CPCM). Excitation energies, respective oscillator strengths and extension coefficients (ε) of the optical absorption for the respective species were evaluated. The geometries of the lowest singlet excited states were optimized with the TD-DFT approach. Fluorescence wavelengths were calculated from the excited state geometries in aqueous solution.

Results and discussion

Various water soluble aromatic molecules containing a phenolic moiety exhibit a pH dependent acid/base equilibrium phenomenon, and thus they have commonly been exploited as pH indicators of aqueous mediums by combination with UV-Vis absorption spectroscopy.[40,41] The pH induced absorbance changes in the visible region, owing to the phenol (neutral)-to-phenolate (anion) interconversion, are beneficial for the optical colorimetric response.[40] The negative charge delocalization in the phenolate anion imparts an additional stability in its excited singlet $(n/\pi)^*$ state resulting in a large red absorption shift, which can be utilized for the colorimetric pH detection. The local interfacial pH was deduced utilizing the acid/base equilibrium of a Schiff-base molecule containing an aromatic phenolic moiety. To anchor the pH-sensing

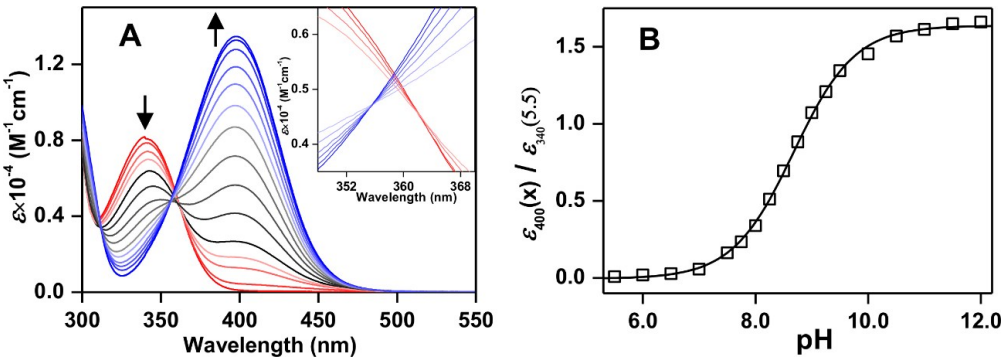

Fig. 1. (A) UV-Vis absorption spectra of Schiff-base molecule AH (5 µM) at different pH (5.5–12.0) values in different 20 mM buffers: (red) Cacodylate, pH 5.5–7.0; (black) tris-HCl, pH 7.0–9.0 and (blue) carbonate/bi-carbonate, pH 9.0–12.0. The increase and decrease in intensities with increase in pH are indicated in arrows. (Inset) Expanded absorption spectra around 360 nm are depicted. Grey spectra are omitted for clarity. (B) Normalized molar extinction coefficient at 400 nm (ε_{400}) at different pH. Each ε_{400} value at different pH is normalized by dividing the extinction coefficient at 340 nm, pH 5.5 (ε_{340} (5.5)).

Schiff-base molecule to the micro-heterogeneous cationic interface electrostatically, 4-amino-4H-1,2,4-triazole containing multiple polar O- and N-centres were reacted with 2-hydroxy-3-(hydroxymethyl)-5-methylbenzaldehyde (Scheme 1).

pH dependent AH acid/base equilibrium in buffer

In the pH-dependent UV-Vis absorption spectra of AH, the 340-nm band of the protonated neutral form (AH) at acidic pH was gradually shifted to a lower energy 400-nm band at higher pH, due to formation of the basic anion form (A^-), where the saturation was observed at pH ~ 12.0 (Fig. 1A). Two isosbestic points were observed at ~ 366 and 356 nm at pH regions 5.5–7.0 and 9.0–12.0, respectively (Inset of Fig. 1A), in the UV-Vis spectra during the conversion of AH to A^-. These results indicate the presence of two ground state phenolate anion conformers with different absorption properties. Therefore, generation of one anionic conformer (A^--I) is exclusive at pH 5.5–7.0, whereas it may further convert into another conformer (A^--II) at pH 9.0–12.0. However, no clear isosbestic point was observed in the absorption spectra at intermediate pH 7.0–9.0, indicating a mixture of both anion conformers at these pH. Approximately 8 nm blue-shift from ~ 408 to 400 nm in the absorption maxima by increase in pH from 7.0 to 12.0 was observed, supporting the above proposition for the generation of two different anion conformers (Fig. 1A). The fluorescence and DFT-based theoretical studies were performed for detailed structural characterization of the two anion conformers (I-A^- and II-A^-) (*vide info*). In spite of the presence of two anion conformers, the normalized 400-nm extension coefficients (ε_{400}) at different pH showed an ideal titration profile with a transition midpoint pK_a at ~ 8.7 (Fig. 1B). Therefore, the acid/base transition can be utilized to determine the pH of aqueous solutions.

AH Acid/base equilibrium in the presence of self-assembled amphiphilic systems

The interaction of AH with self-assembled amphiphilic systems at various pH was monitored by steady state UV-Vis absorption spectrometry (Fig. 2). The intensity of the anionic 408-nm band increased with concomitant decrease in the protonated 340-nm band by an addition of CTAB to AH (5.0 μM) in buffer at pH 6.0–10.0 until a saturation was observed at ~ 5.0 mM CTAB, where an isosbestic point was detected at ~ 365 nm (Fig. S3A, ESI). However, the absorption spectrum of AH did not change by an addition of a similar amount of negatively charged SDS, neutral TX-100 or non-surfactant tetra-n-butylammonium cation (possesses a similar positive group as CTAB), indicating that not only the positive charge but also the micelle forming self-assembling nature are essential for AH to interact with the amphiphilic molecules (Fig. S4, ESI). The intensity of the anionic 408-nm band decreased by increasing the ionic strength of the solution with an addition of saturated concentration of CTAB (5.0 mM) at pH 7.3, showing that AH interacted electrostatically with the cationic interface (Fig. S5, ESI). Saturation of the absorption change was observed at high CTAB

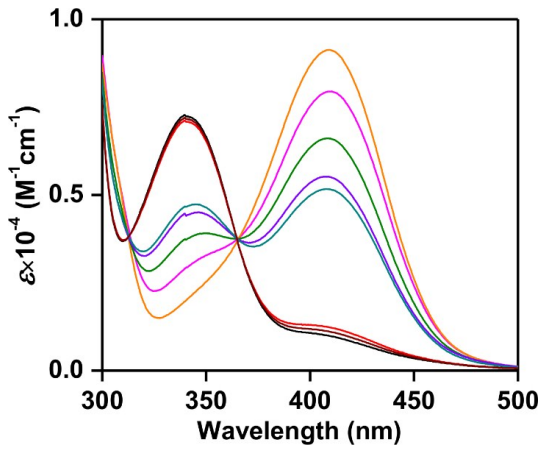

Fig. 2. UV-Vis absorption spectra of AH (5 μM) with different amphiphilic molecules in 20 mM tris-HCl buffer, pH 7.3, at deviation-saturated concentrations of amphiphilic molecules: pink, CTAB (5.0 mM); orange, DDAB (2.0 mM); green, DDAB:DOPC (2:1, total lipid 2.2 mM); dark cyan, DDAB:DOPC (1:1, total lipid 2.5 mM); red, DOPC (3.0 mM), purple, TBP (0.07 mM). The pH of the solution was adjusted to 7.3 by an addition of dilute HCl or NaOH. The spectrum in the presence of tetra-n-butylammonium cation is shown in brown. The spectrum in the absence of tetra-n-butylammonium cation and amphiphilic molecules is shown in black.

concentrations (5.0 mM) well above the critical micelle forming concentration (~ 0.9 mM) irrespective to the pH, indicating that almost all AH molecules interacted with the CTAB micelles (Fig. S3B, ESI). The enhancement extent of the anionic 408-nm band by an addition of CTAB micelles depended on the solution pH, where the largest change was detected near physiological pH ~ 7.3 (Fig. S3B, ESI). The plot of the normalized ε_{408} value (normalized by the 340-nm extinction coefficient at pH 5.5, $\varepsilon_{340}(5.5)$) at deviation-saturated CTAB concentration against the bulk pH exhibited a sigmoidal curve with a transition midpoint at pH ~ 6.9, an apparent pK_a of AH interacting with the amphiphilic molecules (Fig. 3). We attribute the decrease in pK_a by an addition of cationic CTAB micelles to the interaction of AH with the CTAB micelles, causing proton dissociation in AH.

Changes in the AH absorption spectrum (5.0 μM) by an addition of LUVs with different lipid compositions (cationic lipid DDAB (100%), zwitterionic DOPC (100%), DDAB:DOPC (2:1) or DDAB:DOPC (1:1)) were investigated under constant pH conditions (Fig. 2 and S6, ESI). No significant change was observed in the AH absorption spectrum in the presence of 100% DDAB-LUV with different LUV diameters between 50 and 200 nm (Fig. S7, ESI). Gradual increase in the intensity of the 408-nm band with proportionate decrease in that of the 340-nm band in the absorption spectra were detected by increasing the positive DDAB concentration in LUV at a wide range of pH 6.0–10.0 (Fig. S4 and S8, ESI), similar to the effect of CTAB micelles on the AH absorption spectrum (Fig. S3B, ESI). By decreasing the fraction of positive DDAB from 0.5 to 0, the intensities of the 340-nm and 408-nm bands increased and decreased, respectively, for about 50%, whereas the overall lipid concentration to obtain saturation in the LUV-induced absorbance change increased from 2.0 to 2.5 mM

(Fig. S6, ESI). Although the amount of lipid necessary for saturation in the absorption spectra increased for 50% DDAB compare to 100% DDAB, saturation was observed for all the compositions investigated. These results indicate that almost all the AH molecules bound to the positively charged LUV interface at saturated conditions for all the lipid system studies. To assure the AH binding to the LUV interface, binding between AH and LUVs were investigated by determining the residual AH fraction in the bulk phase in the presence of LUV with different lipid compositions (see experimental for details). More than 90% of the AH molecules were attached to LUV for the solution containing 5.0 μM AH and 2.5 mM LUV with different lipid (DDAB and DOPC) compositions (Fig. S9, ESI). These results show that most of the AH molecules were bound to the LUV. The absorbance saturation was observed for the lipid compositions investigated at a wide range of pH, whereas the amount of AH deprotonation varied on pH. The apparent pK_a obtained from the plot of the normalized ε_{408} value at saturated lipid concentration *vs* bulk pH varied by the lipid composition of LUV, presumably due to the change in interfacial positive charges (Fig. 3). The apparent pK_a values for the interface localized AH decreased significantly from 7.6 to 6.7 by increasing the DDAB ratio in the lipid composition from 0 to 0.5 in LUV (Fig. 3, Table 1). This result clearly indicates that more AH deprotonation occurs by increase in the LUV interfacial positive charge.

We extended our investigation to amphiphilic block-co-polymeric compound QPDMA-b-PMMA-b-QPDMA (TBP), which forms a core-shell type micellar structure in aqueous solution.[38] The water/oil interfacial shells are comprised with hydrophilic QPDMA blocks. Cationic quaternary amine and ester groups at the interface are directed to the solvent, whereas the hydrophobic PMMA unit forms the micelle core. The integration magnitude for the 4.37 ppm chemical shift in ^{1}H-NMR spectrum showed that quarterisation of each QPDMA amine of the hydrophilic block, which generates a positive charge at the micellar interface, was about 100% (Fig. S10, ESI).The amount of anion formation increased according to UV-Vis absorption measurements by increasing the concentration of TBP, similar to the case of CTAB micelles and LUV. The intensity increase of the 408-nm absorption band by the interaction with the polymer was ~ 35 and 40% smaller in magnitude at pH 7.3 compared to those by the interaction with CTAB micelles and 100% DDAB-LUV, respectively (Fig. 2). The positive charge density of the polymeric interfacial surface responsible for AH deprotonation may be less compared to those of the interfaces of micelles and LUV. Multiple polar groups in the hydrophilic QPDMA block may distribute in a wide

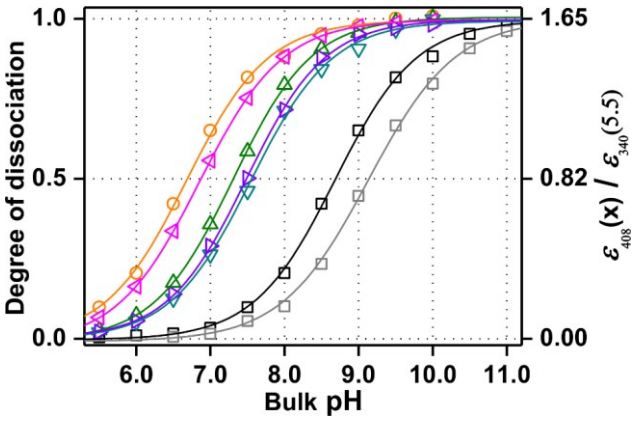

Fig.3 Plots of AH proton dissociation (left y-axis) and normalized molar extinction coefficient at 408 nm (ε_{408}) (right y-axis) against bulk pH in the presence of saturated concentrations of different self-assembled molecules in 20 mM buffer: black, buffer solution without any amphiphilic molecule; gray, 80% ethanol containing buffer; pink, CTAB (5.0 mM); orange, DDAB (2.0 mM); green, DDAB:DOPC (2:1, total lipid 2.2 mM); dark cyan DDAB:DOPC (1:1, total lipid 2.5 mM); purple TBP (0.07 mM). ε at 408 nm at each bulk pH is divided with ε at 340 nm, pH 5.5, in the absence of any amphiphilic molecule.

Table 1: The magnitude of deviation of bulk pH (ΔpH) to obtain the same amount of A^- anions in the absence of cationic self-assembled molecules in 20 mM buffer as those in the presence of self-assembled molecules or ethanol. The anion fractions (f (A^-)) are depicted in brackets respectively.

Bulk pH	ΔpH / f (A^-)						
	[1]Buffer	CTAB	DDAB	DDAB:DOPC (2:1)	DDAB:DOPC (1:1)	TBP	80%-ethanol buffer
[2]8.70	0.00 (0.50)	1.82 (0.96)	1.98 (0.50)	1.40 (0.93)	1.09 (0.87)	1.20 (0.91)	– 0.39 (0.31)
6.0	0.00 (0.02)	1.81 (0.17)	2.00 (0.21)	1.39 (0.08)	1.05 (0.04)	1.21 (0.06)	– 0.40 (0.01)
7.0	0.00 (0.04)	1.81 (0.56)	2.05 (0.64)	1.40 (0.35)	1.05 (0.26)	1.20 (0.28)	– 0.40 (0.02)
8.0	0.00 (0.21)	1.84 (0.88)	2.00 (0.91)	1.39 (0.79)	1.08 (0.69)	1.22 (0.73)	– 0.41 (0.10)
9.0	0.00 (0.65)	1.79 (0.97)	1.98 (0.98)	1.41 (0.96)	1.10 (0.91)	1.20 (0.94)	– 0.39 (0.45)
10.0	0.00 (0.89)	1.84 (0.99)	2.00 (1.00)	1.39 (0.98)	1.04 (0.97)	1.22 (0.99)	– 0.40 (0.80)

[1]The anion fractions in absence of different self-assembled molecules in the bracket are used for the deduction of ΔpH values.
[2]pK_a value for buffer medium.

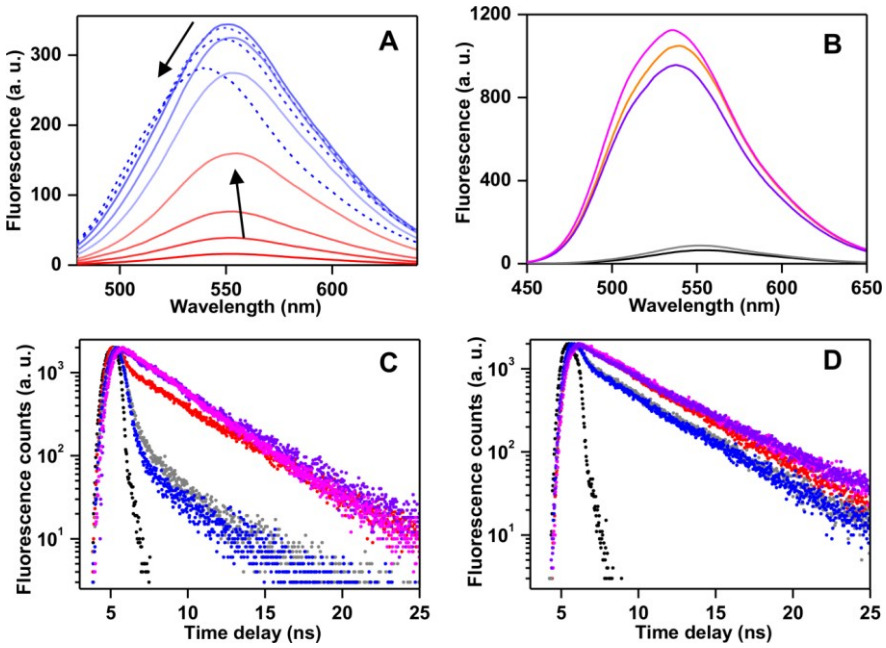

Fig 4. (A) Steady state fluorescence spectra of AH (5 μM) at different pH (5.5–12.0); intensity increase (red and blue) by increasing pH up to 10.0 and subsequent decrease up to pH 12.0 (broken blue) are shown in arrows. (B) Spectra of different self-assembled amphiphilic systems in their respective saturated conditions at pH 7.3; black, buffer without any self-assembled system; pink, CTAB (5.0 mM); orange, DDAB (2.0 mM); purple TBP (0.07 mM) and gray, SDS (5.0 mM). (C,D) Time resolved emission decay curves at different pH in the presence and absence of CTAB/TBP. Excitation and emission wavelengths were 450 and 550 nm, respectively, for (C) and 370 and 500 nm, respectively, for (D): pH, 7.0 (gray), 9.0 (blue), 12.0 (red), 7.0 in the presence of 5.0 mM CTAB (pink) or 0.07 mM TBP (violet). (C,D) Scattering profile is represented in black in (C) and (D).

range and subsequently the thickness of the hydrophilic interface may increase, which results in less AH deprotonation (Scheme 1). However, a same single isosbestic point with a 8-nm red-shift in the absorption spectra by interaction with different self-assembled amphiphilic systems, indicating that only one type of anion (A^--I) was generated at the interface of all amphiphilic systems (Figs. S3A and S6, ESI).

AH Fluorescence studies in the presence of cationic amphiphilic self-assembled systems

Fluorometric investigation was performed in order to obtain details of the pH induced multiple anion formation mechanism of AH. Almost no fluorescent behaviour was detected at ~ pH 5.0, whereas a gradual increase in the steady state fluorescence intensity centred at ~ 550 nm was observed with increase in pH to 9.5, and a subsequent decrease in intensity was observed with a gradual ~ 20-nm blue-shift in the fluorescence maximum by further increase of pH to 12.0 (Fig 4A). To clarify the change of the fluorophoric behaviour pH above 9.5, the 550-nm emission band in the fluorescence excitation spectra was monitored at pH 7.0 and 12.0 (Fig. S11, ESI). Presence of two different fluorophoric anions was indicative by 420- and 370-nm excitations, where the anion conformer A^--I with relatively large fluorescence quantum yield (ϕ_F) was converted gradually with increase in pH to the other anion conformer A^--II with low ϕ_F and a blue-shifted emission. Large increase in the steady state fluorescence intensity and fluorescence anisotropy were induced by an addition of cationic amphiphilic self-assembled systems; the fluorescence anisotropy increased to ~ 0.07 and 0.14 for CTAB and TBP, respectively, from the value ~ 0.01 obtained without addition of any amphiphilic molecule (Fig. 4B, Table S1, ESI). These results are in agreement with the interpretation that AH is anchored to the positively charged interface.

Existence of two different anion conformers was also verified from the bi-exponential transient decay curves with emission lifetimes of ~ 0.35 and 3.5 ns (Fig. 4C, Table S2, ESI). The contribution of the short lifetime (~ 0.35 ns) species in the decay profile increased by increasing pH or changing the excitation wavelength from 450 to 370 nm (Table S2, ESI). These results support the pH dependent steady state fluorescence profile, where the anion conformer A^--I with larger ϕ_F (τ_F = 3.5) gradually converted to the other higher energy ground state conformer A^--II with blue-shifted emission (τ_F = 0.35) by increase in pH. In contrast, a mono-exponential behaviour for AH fluorescence with lifetime of ~ 4.0 ns was observed by excitation at both 370 and 450 nm at various pH (7.0–9.0) in the presence of CTAB and TBP micellar systems. These results strongly indicate that only A^--I was generated when AH interacted with the cationic interface (Fig. 4D, Table S2, ESI), which explains the reason for the large increase in the steady state fluorescence intensity in the presence of cationic amphiphilic self-assembled systems. The single peak at ~ 420 nm in the excitation spectra of A^--I nicely corresponded to the anion absorption peak at 408 in the presence of self-assembling amphiphilic molecules, whereas the mixture of anions A^- (A^--I and A^--II) in the absence of such amphiphilic molecules may be responsible for the blue-shifted absorbance peak at 400 nm, since

Table 2: Electronic excitation wavelength (nm), oscillator strengths (f_{cal}) and extension coefficient of neutral (AH) and two anion conformers (A^--I and A^--II) species obtained by the TD-DFT/B3LYP/6-31G++ calculation on ground state and excited state (*) geometries with CPCM water solvation. The experimentally obtained UV-Vis absorption (Obs/Abs) and fluorescence (Obs/Flu) parameters are depicted for comparison. Associated pH values corresponding to the neutral and anionic forms of AH are shown in brackets.

	Form	Transition	λ, (nm)	f_{cal}	ε×10^{-4} ($M^{-1}cm^{-1}$)
TD-DFT	AH	$S_0 \rightarrow S_1$	358	0.143	0.81
	A^--I	$S_0 \rightarrow S_1$	408	0.379	1.97
	A^--II	$S_0 \rightarrow S_1$	395	0.346	1.91
Obs/Abs	AH (pH 5.5)	$S_0 \rightarrow S_1$	342	-	1.28
	A^- (pH 12.0)	$S_0 \rightarrow S_1$	398	-	2.14
TD-DFT*	A^--I	$S_1 \rightarrow S_0$	529	0.233	-
	A^--II	$S_1 \rightarrow S_0$	495	0.102	-
Obs/Flu	A^- (pH 6.5)	$S_1 \rightarrow S_0$	550	-	-
	A^- (pH 12.0)	$S_1 \rightarrow S_0$	538		-

the excitation band of the anionic A^--II is observe at 370 nm (Fig S6 and S11, ESI).

DFT-based theoretical calculation of two A^- conformers

Structural characterization of the two different anion conformers, A^--I and A^--II, was performed by TD-DFT theoretical calculation.[39] The most probable ground state geometries for neutral AH and its two possible structural isomer anions were optimised to investigate the absorption from the ground state to the singlet excited state in solvent water (Fig. S12, ESI). The excitation energies, oscillator strengths and excited state compositions of the two anion conformers are shown in Table 2. In the calculated UV-Vis optical absorption spectrum, the $S_0 \rightarrow S_1$ vertical electronic transition energies for A^--I, A^--II and neutral AH were 3.17 ev (or 395 nm), 2.80 ev (or 420 nm) and 3.25 ev (or 356 nm), respectively (Table 2). The wavelengths corresponded well to the experimentally observed UV-Vis absorption maximum wavelengths of the anions (~ 400 and ~ 408 nm in the presence and absence of cationic amphiphilic self-assembled molecules, respectively) and neutral species (~ 340 nm), respectively. Similar ε values ~ 1.97×10^4 and 1.91×10^4 $M^{-1}cm^{-1}$ were obtained for A^--I and A^--II respectively, in the calculation. The nature of the pH titration profile for AH is expected to be insensitive to the ratio between the two anion conformers, since the calculated absorption maximum wavelengths and ε values between the two anion conformers were both close to each other (Table 2). For the TD-DFT calculations on optimized excited state geometries, about 30-nm shift of vertical electronic transition and decrease of oscillator strength from 0.23 to 0.10 by comparing A^--I with A^--II were in agreement with the experimentally observed blue shift of the 550-nm emission maximum with decrease in intensity by increasing the pH from 9.0 to 12.0 and increasing the amount of A^--II (Table 2).

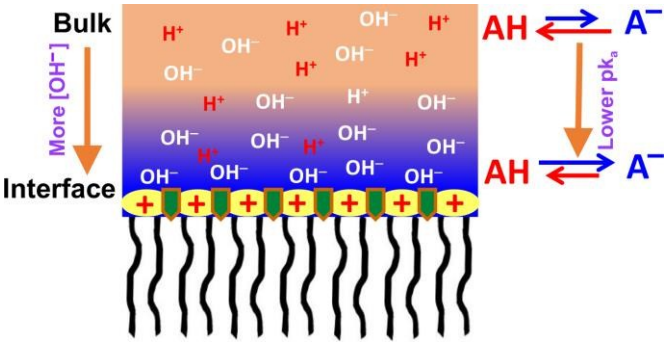

Scheme 2. Schematic representation of the cationic interface induced change of H^+ and OH^- as well as AH/A^- (green) distributions for cationic amphiphilic self-assembled systems. The qualitative nature of the change in the amount of AH dissociation and pK_a difference between the interface and bulk phase are indicated in the right.

Solvent polarity dependent AH dissociation

Solvent polarity has been shown to have a profound role in the acid/base interconversion a molecule, particularly when one of its component is ionic.[42] The amount of ionic form compared to its neutral counterpart increases by stabilization of the ionic species due to increase in the solvent polarity.[42-44] To evaluate the polarity dependent AH dissociation, the equilibrium concentrations of AH and A^- were monitored at various solvent polarities with UV-Vis absorption spectroscopy. The anion A^- concentration decreased ~ 40% by decreasing the solvent polarity of the buffer at pH 9.0 by an addition of ~ 90% (v/v) ethanol (Fig S13, ESI). Since the polarity at the CTAB micellar interface has been reported to be 32.0 D,[43] whereas that of the aqueous solution is ~ 78.0 D, pH dependent acid/base equilibrium titration profile of AH was investigated at pH 6.0–12.0 in the buffer containing 80% (v/v) ethanol with a dielectric constant of ~ 32.0 D (Fig. 3). The pK_a value of AH in the buffer containing 80% (v/v) ethanol was about 0.4 unit higher than that in the aqueous solution (Fig 3, Table 1). These results show that decrease in the polarity at the interface relative to the bulk aqueous phase inhibits the AH dissociation.

Determination of interfacial pH for cationic amphiphilic self-assembled systems

AH was estimated to dissociate in a large amount in the presence of cationic self-assembled systems at bulk pH 6.0–10.0, judging from the change in the relative intensities of the absorbance at 340 and 408 nm attributed to AH and its anion (A^-) forms, respectively (Fig. 2, Table 1). However, a larger amount of AH dissociation in the presence of cationic self-assembled systems was observed by the lowering of apparent pK_a compared to that of the bulk aqueous phase by the change in polarity (Table 1). Therefore, AH becomes more acidic by the polarity effect, when it interacts with the cationic interfaces. Since the AH structure is presumably unchanged upon

binding to the cationic interface, the interfacial micro-phase may be more basic than the corresponding bulk phase, resulting in a higher amount of AH dissociation at the interface. The interfacial positive charge character may increase the basic nature of AH, which can be explained by the following proposition. In the presence of a charged micro-heterogeneous interface, the homogeneity of H^+ and OH^- concentrations may be different between the interfacial and bulk regions.[35] For the cationic self-assembly case, the interfacial positive charge may electrostatically interact with the negatively charged OH^- ions whereas repel the positively charged H^+ and H_3O^+ ions. Therefore, the OH^- ion concentration may become higher at the interface compared to the bulk phase, whereas the H^+ concentration may increase in the bulk phase compared to the interface (Scheme 2). Since the overall volume occupied by the interface is extremely smaller compared to the total effective volume occupied by the bulk phase, the bulk (or intrinsic) pH may remain unchanged. However, the increase in OH^- concentration at the interface may contribute to the higher interfacial (or apparent) pH with respect to the bulk pH (Scheme 2). The higher interfacial basicity may induce AH proton dissociation, and quantitative estimation of AH dissociation can be utilized to estimate the relative deviation of local interfacial pH from its bulk pH in various self-assembled systems. Notably, the proton concentration along the interface depth from the outer to inner region for a self-assembly may vary to some extent by increasing the hydrophobicity as a result of decrease in effective charge density, causing a change in proton dissociation magnitude of AH according to its precise interfacial location. However, irrespective to a wide structural difference among different self-assemblies, AH is expected to locate close to the outer-interface and provide pH information for the outer-interfacial region (Scheme 2), since its interaction with different interfaces containing similar cationic residues is mostly electrostatic in nature.

Protonated AH absorbances at 400 nm or higher wavelength were negligibly small (Fig. 1A), showing that the proton dissociation amount of AH to A^- is proportional to the 408-nm absorbance. Since the observed extension coefficient ratio ($\varepsilon_{408}(x)/\varepsilon_{340}(5.5)$) was 1.65 times as large as the degree of proton dissociation, the normalized extension coefficient ratio by a factor 1.65 represents the degree of proton dissociation (Fig 3). As a result, the intrinsic pH of an aqueous buffer in the absence of self-assembled systems can be directly estimated from the pH-dependent titration profile of AH by analysing the normalized $\varepsilon_{408}(x)/\varepsilon_{340}(5.5)$ or A^- amount (Figs. 1B and 3). However, a lower bulk pH was necessary in order to obtain the same amount of A^- anions in the absence of cationic self-assembled molecules as that in the presence of self-assembled micelles (Fig. 3). These results indicate that the interfacial pH was higher than the bulk pH, since almost all the AH molecules were localised at the self-assembled interface. Therefore, more A^- anions were generated at the interface compared to the bulk phase in the presence of self-assembled systems under same bulk pH of the medium. It can be anticipated that the interfacial pH value is higher by an amount same with the lowering extent of the bulk pH (Δ) induced by the cationic self-assembled systems. However, the observed apparent degree of AH dissociation is not only governed by the interfacial acidity but also the local polarity.[42-44] By the change in polarity from bulk phase (78.0

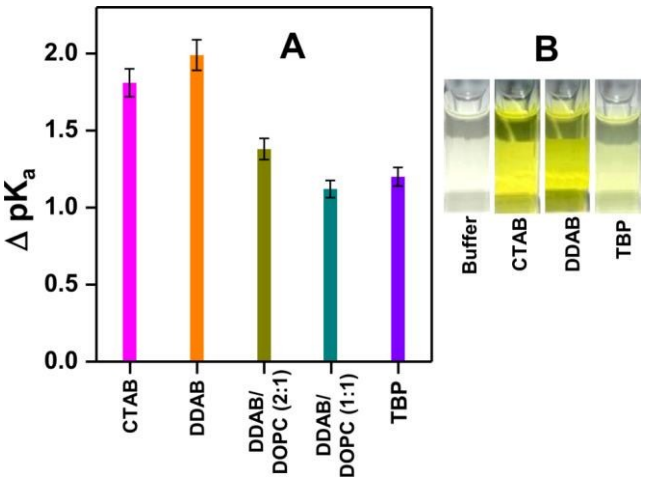

Fig 5. (A) Difference between interface (apparent) and bulk (intrinsic) pK_a (Δ pK_a) for various self-assembled systems. (B) Colorimetric response of AH (20 μM) of various self-assemble systems at pH 7.3. The equivalent of each self-assembled system with respect to AH is the same as that in Fig. 2.

D, pure aqueous buffer) to the interfacial polarity (~ 32.0 D, 80% ethanol containing buffer), approximately 0.4 higher unit of pH was necessary for obtaining the same extent of AH dissociation at pH 6.0–10.0 (Fig. 3, S13, ESI). These results indicate that the decrease in interfacial polarity contributes to less AH dissociation, whereas the higher interfacial pH causes larger extent of AH dissociation.

To estimate the pH effect on AH dissociation at the interface of self-assembled systems, the decrease in A^- anion concentration due to decrease in the interfacial polarity compared to that in its aqueous medium was subtracted from the anion concentration evaluated from the pH-dependent AH dissociation curves in the presence of self-assembled systems. The interfacial/apparent pH would be larger than Δ by 0.4 unit, by considering the enhancement of the A^- anion concentration due to the decrease in polarity. Therefore, the difference between interfacial and bulk pH may be expressed as follows.

$$pH_{intf} - pH_{bulk} = \Delta + 0.4 \quad (1)$$

$$pH_{intf} = pH_{bulk} + \Delta + 0.4 \quad (2)$$

where, pH_{intf} and pH_{bulk} represent the interfacial and bulk pH, respectively. Δ is positive, and its value depends on the self-assembled system. A series of Δ values have been determined for various self-assembled systems at pH 6.0–10.0 (Table 1). Importantly, the Δ value was similar at different pH of the solution for each self-assembled system (Table 1), which indicated that the difference between interfacial and bulk pH is independent to the bulk pH for various amphiphilic self-assembled molecules. We chose the Δ value which corresponded to the difference between intrinsic and apparent pK_a values, where the AH dissociation amount was 0.5 in the presence and absence of self-assembled systems, respectively (Fig. 5, Table 1).

$$\Delta = pK_a(bulk) - pK_a(intf) \quad (3)$$

$pK_a(intf)$ and $pK_a(bulk)$ represent interfacial and bulk pK_a for the self-assembled system. Alternatively, interfacial pH can be expressed as

$$pH_{intf} = pH_{bulk} + pK_a(bulk) - pK_a(intf) + 0.4 \quad (4)$$

The $pK_a(bulk)$ and $pK_a(intf)$ can be determined from the bulk pH dependent titration profile in Fig. 3. The dissociation titration curves

for different self-assemblies can be utilized directly to monitor the local interfacial pH without information on the bulk pH (Fig. 3). However, to obtain information on the deviation between the interface and bulk pH values, the pH relations including the bulk pH as eqs. 1–4 are considered. By using eq. 4, the interfacial pH of CTAB micelles is more basic by a unit of 2.2 compared to that of the corresponding bulk phase pH, whereas the interfacial pH decreases from 2.4 to 1.5 for lipid LUV by decreasing the fraction of positive lipid (DDAB) contents from 1.0 to 0.5 in DDAB:DOPC LUVs (Fig. 5). These results clearly indicate that interfacial positive charges are mostly responsible for higher interfacial pH. For TBP block polymeric micellar systems, a lower Δ+0.4 value (~ 1.6 unit) was obtained, although almost all amine groups in QPDMA were quarternized, i.e., the block copolymer contained positive charge units. The decreases in the interfacial charge density and Δ value for the TBP micellar system compared to those in the CTAB micelles and 100%-DDAB LUV systems were presumably due to the larger polar interface width. Since the absorbance of AH gradually shifts from the UV to visible region with increase in the amount of A^- by increasing the pH, visible colorimetric response is useful for monitoring the pH of the medium. Indeed, less intense yellow colorization was observed for TBP micelles in the visible colorimetric response by addition of AH compared to the bright yellow colorization for CTAB micelles and DDAB-LUVs at same bulk pH of the medium, respectively, strongly indicating less formation of A^- anions due to less increase in the interfacial pH compared to the bulk pH for the polymeric system (Fig. 5B). Since the apparent pK_a in the presence of self-assembled systems is very close to the physiological pH value (Fig. 3), detection of interfacial pH for various physiological systems may be possible by utilizing the present interface selective pH sensing probe. However, the suitability for the detection of unknown intrinsic/apparent pH in a pH range of 5.5–12.0 was confirmed by observing reversible interconversion between protonated AH and deprotonated A^- species, where the absorption spectrum in pure aqueous buffer at pH 5.5 was found identical to that at the same pH achieved by increasing the pH value from 5.5 to 12.0 and subsequently reversing back the pH value to 5.5 by consecutive addition of diluted NaOH and HCl, respectively (Fig. S14, ESI).

Conclusions

We developed a new UV-Vis absorption method to estimate the deviation of interfacial pH from its bulk pH in cationic amphiphilic self-assembled systems, such as CTAB micelles, LUVs of different lipid compositions and block polymeric micelles, by investigating the acid/base equilibrium of a Schiff-base molecule AH which interacted selectively at the interfaces. Effect of AH in the bulk phase during estimation of its interfacial dissociation was eliminated by the large AH binding affinity to the cationic interfaces. Modulation of the interfacial pH from bulk pH was detected at a wide range of pH 6.0–10.0, since the cationic self-assembled systems induced AH deprotonation, which correlated with the interfacial basic character. Fluorescence studies were utilized to observe pH dependent interconversion between the two isomeric anion conformers (A^--I and A^--II) of AH in buffer, whereas formation of A^--I occurred exclusively in the presence of cationic micelles and vesicles. The absorption parameters of deprotonated and protonated forms of AH were identified by theoretical calculations, showing that the calculated absorption maximum wavelengths and ε values between the two anion conformers are both close to each other. The experimental simplicity of the present interfacial pH detection method may provide an opportunity for the detection of interfacial pH of various biologically important interfaces.

Acknowledgements

This work was supported by Research Projects (SB/FT/CS-089/2013) (PPP) and UGC (ERO) MRP (PSW-196/13-14) (AR). SD acknowledges UGC (ERO) MRP, for research Grant (PSW-197/13-14). YS acknowledges UGC for JRF fellowship.

Notes and references

1 C. H. Foyer, *Plant Cell*, 2005, **17**, 1866.
2 W. A. Prinz, *J. Cell Biol*, 2014, **205**, 759.
3 D. Sanders, U. Hansen and C. L. Slayman, *Proc. Natl. Acad. Sci. USA*, 1981, **78**, 5903.
4 W. Aoi and Y. Marunaka, *BioMed. Res. Int.*, 2014, **2014**, 8.
5 A. Roos and W. F. Boron, *Physiol. Rev.*, 1981, **61**, 296.
6 R. A. Gottlieb and A. Dosanjh, *Proc. Natl. Acad. Sci. USA.*, 1996, **93**, 3587.
7 D. P. Sala, D. C. Escobar and F. Mollinedo, *J. Biol. Chem.*, 1995, **270**, 6235.
8 D. L. Gossmann, L. huc and V. Lecureur, *Cell Death and Differ.*, 2004, **11**, 953.
9 S. Matsuama and J. C. Reed, *Cell Death and Differ.,* 2000, **7**, 1155.
10 S. Katayama, I. Nakase, Y. Yano, T. Murayama, Y. Nakata, K. Matsuzaki and S. Futaki, *Biochimica et Biophysica Acta,* 2013 **1828**, 2134.
11 H. Lodish, A. Berk, S. L. Zipursky, P. Matsudaira, D. Baltimore and J. Darnell, *TRENDS in Cell Biology*, 2005, **15**, 396.
12 M. Kraub and V. Haucke, *EMBO Rep.,* 2007, **8**, 241.
13 M. Schindler, S. Grabski, E. Hoff and S. M. Simon, *Biochemistry*, 1996, **35**, 2811.
14 M. Montrose, T. Friedrich and H. Murer, *J. Membr. Biol*., 1987, **97**, 63.
14 H. Izumi, T. Torigoe, H. Ishiguchi, H. Uramoto, Y. Yoshida, M. Tanabe, T. Ise, T. Murakami, T. Yoshida, M. Nomoto and K. Kohno, *Cancer Treat. Rev.*, 2003, **29**, 541.
15 P. Swietach, R. D. V. Jones, A. L. Harris and A. Hulikova, *Phil. Trans. R. Soc. B*., 2014, **369**, 1638.
16 T. A. Davies, R. E. Fine, R. J. Johnson, C. A. Levesque, W. H. Rathbun, K. F. Seetoo, S. J. Smith, G. Strohmeier, L. Volicer, L. Delva and E. R. Simons, *Biochem. Biophys. Res. Commun.*, 1993, **194**, 537.
17 S. Hoefgen, S. O. Dahms, K. Oertwig and M. E. Than, *J. Mol. Biol.,* 2015, **427**, 433.
18 D. Wijesinghe, M. C. M. Arachchige, A. Lu, Y. K. Reshetnyak and O. A. Andreev, *Sci. Rep*., 2013, **3**, 3560.
19 A. Chenal, G. Vvernier, P. Savarin, N. A. Bushmarina, A. Geze, F. Guillain, D. gillet and V. Forge, *J. Mol. Biol.,* 2005, **349**, 890.
20 C. V. Ballmoos, A. Wiedenmann and P. Dimroth, *Annu. Rev. Biochem*., 2009, **78**, 649.
21 D. Schmaljohann, *Adv. Drug Deliv. Rev.*, 2006, **58**, 1655.
22 K. M. Huh, H. C. Kang, Y. J. Lee, and Y. H. Bae, *Macromol. Res.*, 2012, **20,** 224.
23 I. Nakase and S. Futaki, *Sci. Rep.*, 2015, **5**, 10112.
24 S. Akerman, K. Akerman, J. Karppi, P. Koivu, A. Sundell, P. Paronen and K. Jarvinen, *Eur. J. Pharm. Sci.*, 1999, **9**, 137.
25 C. Peetla, A. Stine and V. Labhasetwar, *Mol. Pharm*., 2009, **6**, 1264.

26 P. Mukerjee and K. Banerjee, *J. Phys. Chem.*, 1964, **68**, 35674.
27 C. G. Knight and T. Stephens, *Biochem. J.* 1989, **15**, 258, 683.
28 F. R. Beierlein, A. M. Krause, C. M. Jager, P. Fita, E. Vauthey and T. Clark, *Langmuir,* 2013, **29**, 11898.
29 C. J. Drummond, F. Grieser and T. W. Healy, *J. Chem. Soc.*, 1989, **85**, 561.
30 A. Mohr, T. P. Vila, H. G. Korth, H. Rehage and R. Sustmann, *Chem Phys Chem*, 2008, **9**, 2397.
31 F. M. A. Altalbawy and E. A. M. Al-Sherbini, *Asian. J. Chem*., 2013, **25,** 6181.
32 M. A. Voinov, I. A. Kirilyuk and A. I. Smirnov, *J. Phys. Chem. B*, 2009, **113**, 3453.
33 D. Maouyo, S. CHU, and M. H. Montrose, *Am. J. Physiol.,Cell Physiol., 2000,* **278,** C973.
34 S. Yamaguchi, K. Bhattacharyya and T. Tahara, *J. Phys. Chem. C,* 2011, **115**, 4168.
35 A. Kundu, S. Yamaguchi and T. Tahara, *J. Phys. Chem. Lett*., 2014, **5**, 762.
36 U. Chatterjee, S. K. Jewrajka and B. Mandal, *Polymer*, 2005, **46**, 1575.
37 E. Lambert, B. Chabut, S. C. Noblat, A. Deronzier, G. Chottard, A. Bousseksou, J. P. Tuchagues, J. Laugier, M. Bardet and J. M. Latour, *J. Am. Chem. Soc.*, 1997, **119,** 9424.
38 Y. Sarkar, S. Das, R. Datta, S. Chattopadhyay, A. Ray and P. P. Parui, *RSC Adv.,* 2015, **5**, 51875.
39 M. J. Frisch, et al., *Gaussian 09 Rev*. *A.1*, Gaussian Inc., Wallingford CT, 2009.
40 U. C. Saha, K. Dhara, B. Chattopadhyay, S. K. Mandal, S. Mondal, S. Sen, M. Mukherjee, S. V. Smaalen, and P. Chattopadhyay, *Org. Lett*, 2011, **13**, 4510.
41 J. T. Miao, C. Fan, X. Y. Shi, R. Sun, Y. J. Xu and J. F. Ge, *Analyst*, 2014, **139**, 6290.
42 M. S. Fernandez and P. Fromherz, *J. Phys. Chem.*, 1977, **81**, 1755.
43 K. A. Zacharlasse, V. P. Nguyen and B. Koranklewicr, *J. Phys. Chem.*, 1981, **85**, 2676.
44 C. J. Drummond, F. Grieser and T. W. Healy, *Farad. Discuss. Chem. Soc.*, 1986, **81**, 95.

Graphical Abstract

A simple interfacial pH detection method for cationic amphiphilic self-assemblies utilizing a Schiff-base molecule

YeasminSarkar, Sanju Das, Ambarish Ray, Suresh Kumar Jewrajka, Shun Hirota and Partha Pratim Parui*

A simple pH-sensing method for cationic micelle and vesicle interfaces is introduced, utilizing a Schiff-base molecule AH. The change in the AH proton dissociation between interface and bulk was monitored to evaluate the amount of the interfacial pH deviation from the bulk pH.